LETTERS
PUBLISHED ONLINE: 9 OCTOBER 2011 | DOI: 10.1038/NPHYS2114

nature physics

Tunable metal–insulator transition in double-layer graphene heterostructures

L. A. Ponomarenko[1], A. K. Geim[1,2], A. A. Zhukov[2], R. Jalil[2], S. V. Morozov[1,3], K. S. Novoselov[1], I. V. Grigorieva[1], E. H. Hill[2], V. V. Cheianov[4], V. I. Fal'ko[4], K. Watanabe[5], T. Taniguchi[5] and R. V. Gorbachev[2]*

Disordered conductors with resistivity above the resistance quantum h/e^2 should exhibit an insulating behaviour at low temperatures, a universal phenomenon known as a strong (Anderson) localization[1–3]. Observed in a multitude of materials, including damaged graphene and its disordered chemical derivatives[4–10], Anderson localization has not been seen in generic graphene, despite its resistivity near the neutrality point reaching $\approx h/e^2$ per carrier type[4,5]. It has remained a puzzle why graphene is such an exception. Here we report a strong localization and the corresponding metal–insulator transition in ultra-high-quality graphene. The transition is controlled externally, by changing the carrier density in another graphene layer placed at a distance of several nm and decoupled electrically. The entire behaviour is explained by electron–hole puddles that disallow localization in standard devices but can be screened out in double-layer graphene. The localization that occurs with decreasing rather than increasing disorder is a unique occurrence, and the reported double-layer heterostructures presents a new experimental system that invites further studies.

Resistivity values $\approx h/e^2$ indicate that the electron mean free path l is shorter than the Fermi wavelength λ_F, so that quantum interference becomes a dominant feature in electron diffusion, leading to Anderson localization in the absence of phase-breaking processes at low temperatures (T). The scope of this phenomenon extends beyond electronic systems—into optical and acoustic phenomena as well[1–3]—but not generic graphene, which remains metallic at liquid-helium T (refs 4,5) and exhibits only a weak T dependence that can be explained by phonons and thermally excited carriers[11]. Earlier theoretical studies have suggested that Dirac electrons can evade localization for certain types of disorder[3,12–15], with the extreme example being graphene subjected to a smooth Coulomb potential[16,17]. However, for generic disorder that involves scattering between the two graphene valleys, the localization is expected to be unavoidable[3,18,19]. Experiments do not show this.

In this Letter, we describe a double-layer electronic system made of two closely-spaced but electrically isolated graphene monolayers sandwiched in boron nitride. In the following, the two layers in the double layer graphene (DLG) heterostructure are referred to as the studied and control layers. At low doping n_C in the control layer, the studied layer exhibits the standard behaviour with a minimum metallic conductivity of $\sim 4e^2/h$. However, for $n_C > 10^{11}\,\mathrm{cm}^{-2}$, the resistivity ρ of the studied layer diverges near the neutrality point (NP) at $T < 70\,\mathrm{K}$. This divergence can be suppressed by a small perpendicular field $B < 0.1\,\mathrm{T}$, which indicates that this is an interference effect rather than a gap opening. We attribute the metal–insulator transition (MIT) to the recovery of an intrinsic behaviour such that graphene exhibits Anderson localization if its ρ reaches values of $\approx h/e^2$ per carrier type. Normally, this intrinsic MIT is obscured by charge inhomogeneity in the form of electron–hole puddles[20–24]. Within each puddle, graphene is sufficiently away from the NP and remains metallic. Then, resistivity of the percolating electron–hole system with leaking p–n boundaries[16,17] assumes a value of $\sim h/e^2$ with little T dependence (conceptually this value has little in common with the similar value required for Anderson localization)[23,24]. The control layer can screen out the fluctuating background potential and suppress electron–hole puddles, revealing the intrinsic properties at the NP. This reconciles the metallic behaviour normally observed in graphene with the localization expected for large ρ and supports the idea that the minimum conductivity that tends to assume values close to $4e^2/h$ is due to electron–hole puddles[23,24].

The studied devices were fabricated by sandwiching two graphene monolayers with thin hexagonal-BN crystals. In a multistep procedure, described in the Supplementary Information, a graphene monolayer was transferred onto a 20–30 nm thick BN crystal that was first prepared on top of an oxidized Si wafer. Then, the graphene was covered with another BN crystal (spacer), which was followed by transfer of the second graphene layer. Both layers were shaped into multiterminal devices aligned above each other and having separate electrical contacts (Fig. 1a). Individual steps were similar to those described in refs 25,26 but the whole fabrication process involved three dry transfers and alignments, four nonconsecutive rounds of electron-beam lithography, three rounds of plasma etching and two separate metal depositions. The resulting DLG heterostructures are schematically shown in Fig. 1a (for images, see Supplementary Information). We made several such devices with channel widths of 1–2 μm. They exhibited μ of 30 –120 $\times 10^3\,\mathrm{cm}^2\,\mathrm{V}^{-1}\,\mathrm{s}^{-1}$ and little chemical doping. The bottom layer encapsulated in BN always had higher μ and changed little after exposure to air[26] whereas the quality of the top layer gradually decayed. For this particular study, we employed three multiterminal devices with sufficiently thick BN spacers to avoid any detectable tunnel current between graphene layers (<0.1 nA). The spacers had thicknesses $d \approx 4$, 12 and 16 nm. All the devices exhibited a similar MIT behaviour, although the insulating state was much more pronounced for devices with smaller d and higher μ, as described below.

[1]School of Physics and Astronomy, University of Manchester, Manchester M13 9PL, UK, [2]Manchester Centre for Mesoscience and Nanotechnology, Manchester M13 9PL, UK, [3]Institute for Microelectronics Technology, 142432 Chernogolovka, Russia, [4]Physics Department, University of Lancaster, Lancaster LA1 4YB, UK, [5]National Institute for Materials Science, 1-1 Namiki, Tsukuba, 305-0044, Japan. *e-mail: blizza@gmail.com.

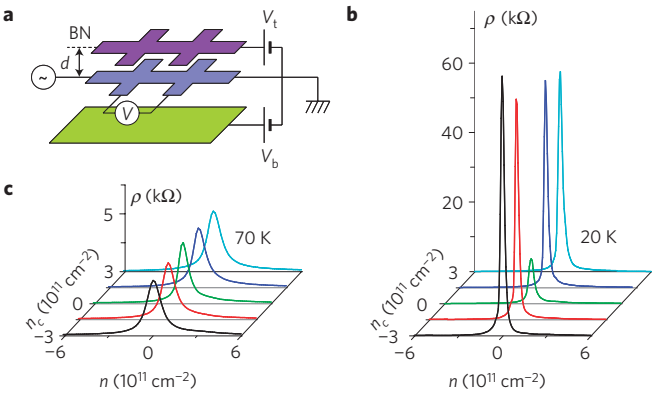

Figure 1 | Electron transport in graphene–BN heterostructures. **a**, Schematic view of our heterostructure devices and measurement geometry. **b**,**c**, ρ as a function of n in the studied graphene layer for different doping n_C of the control layer at two temperatures. The device has a 4 nm BN spacer.

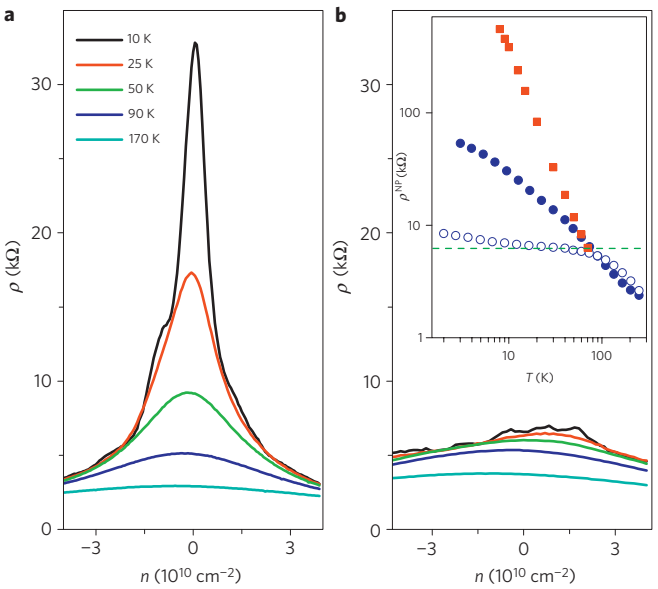

Figure 2 | Resistivity of the studied layer at different T for high and low doping of the control layer. a,**b**, Correspond to $n_C \approx 3 \times 10^{11}$ cm^{-2} and zero n_C, respectively. Here, we have chosen to plot data for $d \approx 12$ nm. For our thinnest spacer (≈4 nm), ρ^{NP} becomes very large at low T (inset) and continuous curves $\rho(n)$ are difficult to measure because of crosstalk nonlinearities (Supplementary Information). The inset shows the T dependence of ρ^{NP} for the device in the main figure at both n_C (open and filled circles) and for the 4 nm device at $n_C \approx 5 \times 10^{11}$ cm^{-2} (squares). The dashed line indicates the threshold value for Anderson localization, $\rho = h/4e^2$.

With reference to Fig. 1a, we employed the following scheme of measurements. A voltage V_t was applied between the graphene layers, and this electrically doped both of them with carriers of the opposite sign. The bottom layer could also be gated by a voltage V_b applied to the Si wafer. Because of the low density of states, graphene can provide only a partial screening and, therefore, V_b induced carriers in the top layer as well. This influence was weaker than on the bottom layer and depended on n in the latter. By measuring the Hall resistivity ρ_{xy} we could determine n in each of the layers (Supplementary Information). We usually fixed V_t to define a nearly constant n in the top layer and swept V_b to vary n in the bottom layer. Normally, we studied the higher-μ bottom layer and used the top layer as control. In this configuration, the insulating state reached higher ρ. If the studied and control layers were swapped, the behaviour remained qualitatively the same (Supplementary Information) but lower μ resulted in lower ρ of the insulating state.

Our main result is illustrated by Fig. 1, which shows two sets of standard curves $\rho(n)$ for the studied layer at different n_C. At 70 K, the control layer has little effect on the studied layer, and all the curves in Fig. 1b look no different from those observed in the standard devices[4] or for graphene on BN (GBN; ref. 25). However, at low T and for high doping of the control layer ($n_C > 10^{11}$ cm^{-2}), graphene exhibits a radically different behaviour (Fig. 1c). In this regime, ρ at the NP acquires a strong T dependence and easily overshoots the threshold value of h/e^2. To elucidate this observation, Fig. 2 shows further examples of $\rho(n, T)$ for high and low doping of the control layer. In the case of large n_C (Fig. 2a), ρ exhibits an insulating T dependence. In contrast, zero n_C results in a much weaker T dependence that can be explained by thermally excited carriers (Fig. 2b). Outside a relatively narrow interval $|n| \leq 10^{10}$ cm^{-2} and above 70 K, the behaviour of graphene was practically independent of n_C.

The T dependence of the maximum resistivity at the NP, ρ^{NP}, is shown in more detail in the inset of Fig. 2b for zero and high doping of the control layer. The insulating state is more pronounced for $d = 4$ nm but remains clear also for the 12 nm device (note the logarithmic scale). For $d = 4$ nm and below 4 K, ρ^{NP} could reach into the MΩ range (Supplementary Information), an increase by 2–3 orders of magnitude with respect to the standard behaviour. The high-ρ regime is found to be difficult to probe because of a strong nonlinearity caused by a crosstalk between the measurement current and V_t, the effect specific to DLG devices with small d (see Supplementary Information). To assure the linear response in this regime, we had to measure I–V curves at every gate voltage and, to avoid these difficulties, we limited our studies mostly to $T > 4$ K and $\rho^{NP} < 100$ kΩ.

The influence of the adjacent layer immediately invites one to consider interlayer Coulomb interactions. Indeed, the relevant energy scale is $e^2/\varepsilon d \sim 50$ meV, that is, the interactions may be a significant factor ($\varepsilon \approx 5$ is BN's dielectric constant). For example, one can imagine that the interactions open an excitonic-like gap at the Dirac point. We have ruled out this possibility by magnetic field measurements. In the gapped case, B is expected to enhance the confinement and, hence, the binding energy. In contrast, our devices exhibit a pronounced negative magnetoresistance in non-quantizing B (Fig. 3). The insulating behaviour is suppressed in characteristic $B^* \approx 10$ mT (Fig. 3), well below the onset of Landau quantization. Figure 3 also shows that the MIT is again confined to $|n| \leq 1 \times 10^{10}$ cm^{-2}.

Another interesting observation is that the insulating state has always developed at $\rho > h/4e^2$ (Figs 1–3). This is seen most clearly in the inset of Fig. 2, where the curves depart from each other above the dashed line marking $h/4e^2$. In the insulating state, ρ^{NP} is found to follow a power-law dependence $1/T^{\nu}$, where ν varied from sample to sample, reaching a value close to two in the device with $d \approx 4$ nm. The characteristic T at which the insulating state started to develop can be attributed to the fact that above 70 K the concentration of excited carriers at the NP exceeded $\approx 10^{10}$ cm^{-2}, beyond which no MIT could be observed even at low T.

The suppression of the MIT by non-quantizing B is a clear indication that localization plays an important role, such that B breaks down the time-reversal symmetry and destroys the interference pattern that developed due to self-intersecting trajectories[1–3]. The strong localization scenario is also consistent with the onset of the insulating state at $\rho^{NP} \approx h/4e^2$, which corresponds to the resistivity quantum per carrier type. However, localization in graphene cannot possibly be explained without intervalley scattering[3,18,19]. A tempting line of argument would be to invoke charge fluctuations in the control layer to explain its influence on the studied layer. However,

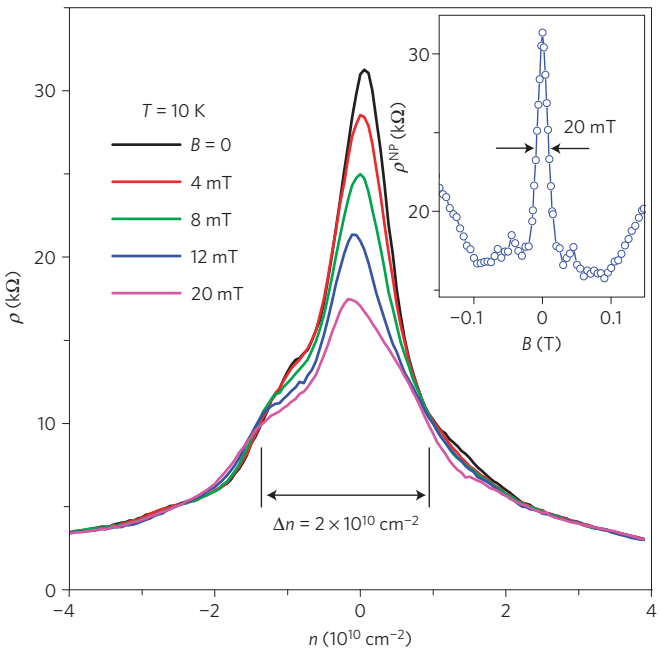

Figure 3 | Resistivity of the studied layer in the insulating regime at various *B*. $d = 12$ nm; $n_C \approx 3 \times 10^{11}$ cm^{-2}. At low T, $\rho(n)$ exhibits pronounced 'mesoscopic' fluctuations (for example, the left shoulder in this figure) which develop further with decreasing T and are probably due to macroscopic charge inhomogeneity. Inset—detailed B dependence of ρ^{NP} for the case shown in the main figure.

this contradicts the fact that μ can increase notably at high n_C, that is, graphene exhibits higher quality rather than extra scattering if the control layer is strongly doped (Supplementary Information). Moreover, the Coulomb interaction between the layers is generally expected to become less efficient with decreasing T and increasing n_C (ref. 27), which is exactly opposite to what we observe. Finally, an interlayer scattering mechanism can be ruled out by the fact that any interaction potential created by carriers in the control layer and acting on the studied layer varies at distances of $\sim d \gg a$ (a is the lattice constant), whereas the fast components needed for intervalley scattering depend exponentially on a/d (ref. 28).

To explain the MIT, we assume a small amount of intervalley scatterers already present in our devices. They could be either some of the defects that limit μ (for example, strong adsorbates)[29] or, alternatively, the intervalley scattering can arise because of the atomic-scale potential created by BN. In both cases, this can break down the symmetry between the carbon sublattices and act as a source of intervalley scattering. Because the insulating state is observed only for $|n| \leq 10^{10}$ cm^{-2} and the process responsible for Anderson localization should provide a mean free path of about $\lambda_F = (4\pi/n)^{1/2}$, we can estimate the intervalley scattering length l_{iv} as ~0.1 μm.

Furthermore, $B^* \sim 10$ mT yields a spatial scale $(\phi_0/B^*)^{1/2} \approx 0.5$ μm, which corresponds to a flux quantum $\phi_0 = h/e$ enclosed by diffusive trajectories. This scale is significantly larger than the mean free path $l \leq 0.1$ μm estimated for the relevant interval of $n \leq 10^{10}$ cm^{-2} and, therefore, this justifies the use of diffusive transport concepts. Fitting the magnetoresistance curves, such as in Fig. 3, by the weak localization formulas[19,30] (although mentioning that those are applicable to small rather than large changes in ρ) yields two other spatial scales. One corresponds to the onset of magnetoresistance (~1 mT) and yields the phase-breaking length of a few μm at liquid-helium T, which is typical for graphene[30,31]. The other scale (≈0.1 μm) is given by $B \approx 0.1$ T, where the magnetoresistance saturates, before changing its sign from negative to positive. The latter scale could be due to the onset of intervalley scattering[18,19,31], which agrees well with the value l_{iv} determined from the above analysis of the MIT.

The proposed scenario for the MIT can be considered routine for any high-ρ metallic system at low T, including the previously studied damaged graphene, which contains a large amount of short-range, intervalley scatterers[7–10]. Quality graphene has been the only known exception until now. Therefore, the question should be turned around and it should be asked why there is no MIT in the standard graphene devices or DLG at low n_C and why the MIT becomes pronounced only in our ultra-high-quality graphene. The latter seemingly contradicts the very notion of Anderson localization. The puzzle has a straightforward resolution if we attribute this behaviour to the presence of electron–hole puddles[4,23,24].

In graphene on SiO_2, the puddles contain carriers in typical $n \sim 10^{11}$ cm^{-2} (ref. 20). In GBN, puddles are larger and shallower[21,22] but, within each puddle, n is still high enough ($>10^{10}$ cm^{-2}) to move the system away from the MIT. The resistivity of such an inhomogeneous system is then determined by inter-puddle ballistic transport with $\rho \sim h/4e^2$ (refs 23,24). The recovery of the MIT can be expected if n within the electron–hole puddles decreases below the localization threshold (≈10^{10} cm^{-2} in our case). Accordingly, we attribute the influence of the control layer to the fact that at high n_C it screens out the background potential, making puddles shallower, as our numerical modelling shows (see Supplementary Information). Experimentally, this is also the case, as seen from Hall measurements where the transition region in ρ_{xy} (between electron- and hole-regimes) narrows at high n_C (Supplementary Information). Further work is required to understand the underlying physics in detail and, especially, the mechanism of intervalley scattering and a possible role of the atomic washboard created by BN.

Received 23 June 2011; accepted 9 September 2011; published online 9 October 2011

References

1. Kramer, B. & Mackinnon, A. Localization—theory and experiment. *Rep. Prog. Phys.* **56,** 1469–1564 (1993).
2. Imada, M., Fujimori, A. & Tokura, Y. Metal–insulator transitions. *Rev. Mod. Phys.* **70,** 1039–1263 (1998).
3. Evers, F. & Mirlin, A. D. Anderson transitions. *Rev. Mod. Phys.* **80,** 1355–1417 (2008).
4. Geim, A. K. & Novoselov, K. S. The rise of graphene. *Nature Mater.* **6,** 183–191 (2007).
5. Castro Neto, A. H. *et al.* The electronic properties of graphene. *Rev. Mod. Phys.* **81,** 109–162 (2009).
6. Gomez-Navarro, C. *et al.* Electronic transport properties of individual chemically reduced graphene oxide sheets. *Nano Lett.* **7,** 3499–3503 (2007).
7. Zhou, S. Y., Siegel, D. A., Fedorov, A. V. & Lanzara, A. Metal to insulator transition in epitaxial graphene induced by molecular doping. *Phys. Rev. Lett.* **101,** 086402 (2008).
8. Bostwick, A. *et al.* Quasiparticle transformation during a metal–insulator transition in graphene. *Phys. Rev. Lett.* **103,** 056404 (2009).
9. Elias, D. C. *et al.* Control of graphene's properties by reversible hydrogenation: Evidence for graphane. *Science* **323,** 610–613 (2009).
10. Chen, J. H. *et al.* Defect scattering in graphene. *Phys. Rev. Lett.* **102,** 236805 (2009).
11. Adam, S. & Das Sarma, S. Boltzmann transport and residual conductivity in bilayer graphene. *Phys. Rev. B* **77,** 115436 (2008).
12. Nersesyan, A. A., Tsvelik, A. M. & Wenger, F. Disorder effects in 2-dimensional d-wave superconductors. *Phys. Rev. Lett.* **72,** 2628–2631 (1994).
13. Ludwig, A. W. W., Fisher, M. P. A., Shankar, R. & Grinstein, G. Integer quantum Hall transition—an alternative approach and exact results. *Phys. Rev. B* **50,** 7526–7552 (1994).
14. Hatsugai, Y., Wen, X. G. & Kohmoto, M. Disordered critical wave functions in random-bond models in two dimensions: Random-lattice fermions at $E = 0$ without doubling. *Phys. Rev. B* **56,** 1061–1064 (1997).
15. Ryu, S. & Hatsugai, Y. Singular density of states of disordered Dirac fermions in chiral models. *Phys. Rev. B* **65,** 033301 (2002).
16. Katsnelson, M. I., Novoselov, K. S. & Geim, A. K. Chiral tunnelling and the Klein paradox in graphene. *Nature Phys.* **2,** 620–625 (2006).

17. Cheianov, V. V. & Fal'ko, V. I. Selective transmission of Dirac electrons and ballistic magnetoresistance of n–p junctions in graphene. *Phys. Rev. B* **74,** 041403 (2006).
18. Aleiner, I. L. & Efetov, K. B. Effect of disorder on transport in graphene. *Phys. Rev. Lett.* **97,** 236801 (2006).
19. McCann, E. *et al.* Weak-localization magnetoresistance and valley symmetry in graphene. *Phys. Rev. Lett.* **97,** 146805 (2006).
20. Martin, J. *et al.* Observation of electron–hole puddles in graphene using a scanning single-electron transistor. *Nature Phys.* **4,** 144–148 (2008).
21. Xue, J. M. *et al.* Scanning tunnelling microscopy and spectroscopy of ultra-flat graphene on hexagonal boron nitride. *Nature Mater.* **10,** 282–285 (2011).
22. Decker, R. *et al.* Local electronic properties of graphene on a BN substrate via scanning tunnelling microscopy. *Nano Lett.* **11,** 2291–2295 (2011).
23. Adam, S., Hwang, E. H., Galitski, V. M. & Das Sarma, S. A self-consistent theory for graphene transport. *Proc. Natl Acad. Sci. USA* **104,** 18392–18397 (2007).
24. Cheianov, V. V., Fal'ko, V. I., Altshuler, B. L. & Aleiner, I. L. Random resistor network model of minimal conductivity in graphene. *Phys. Rev. Lett.* **99,** 176801 (2007).
25. Dean, C. R. *et al.* Boron nitride substrates for high-quality graphene electronics. *Nature Nanotech.* **5,** 722–726 (2010).
26. Mayorov, A. S. *et al.* Micrometer-scale ballistic transport in encapsulated graphene at room temperature. *Nano Lett.* **11,** 2396–2399 (2011).
27. Tse, W. K., Hu, B. Y. K. & Das Sarma, S. Theory of Coulomb drag in graphene. *Phys. Rev. B* **76,** 081401 (2007).
28. Ponomarenko, L. A. *et al.* Effect of a high-κ environment on charge carrier mobility in graphene. *Phys. Rev. Lett.* **102,** 206603 (2009).
29. Ni, Z. H. *et al.* On resonant scatterers as a factor limiting carrier mobility in graphene. *Nano Lett.* **10,** 3868–3872 (2010).
30. Tikhonenko, F. V., Horsell, D. W., Gorbachev, R. V. & Savchenko, A. K. Weak localization in graphene flakes. *Phys. Rev. Lett.* **100,** 056802 (2008).
31. Tikhonenko, F. V., Kozikov, A. A., Savchenko, A. K. & Gorbachev, R. V. Transition between electron localization and antilocalization in graphene. *Phys. Rev. Lett.* **103,** 226801 (2009).

Acknowledgements

We thank M. Katsnelson, A. MacDonald and A. C. Neto for useful discussions. This work was supported by the Engineering and Physical Sciences Research Council (UK), the Royal Society, the Office of Naval Research, the Air Force Office of Scientific Research and the Körber Foundation.

Author contributions

R.V.G. designed the experiments; L.A.P. and S.V.M. carried out measurements; R.V.G. and R.J. fabricated the devices; L.A.P., R.V.G. and A.K.G. carried out data analysis; L.A.P., A.A.Z. and A.K.G. wrote the article. All the authors contributed to discussions. L.A.P. and R.V.G. contributed to the work equally.

Additional information

The authors declare no competing financial interests. Supplementary information accompanies this paper on www.nature.com/naturephysics. Reprints and permissions information is available online at http://www.nature.com/reprints. Correspondence and requests for materials should be addressed to R.V.G.

nature physics

SUPPLEMENTARY INFORMATION

DOI: 10.1038/NPHYS2114

Tunable metal-insulator transition in double-layer graphene heterostructures

L. A. Ponomarenko *et al.*

#1 *Sample fabrication*

The studied devices (see Fig. S1) were fabricated by using the following multistep procedure. First, relatively thick (20-30 nm) crystals of hexagonal BN (hBN) were cleaved on top of an oxidized Si wafer (SiO_2 had thickness of either ≈90 or ≈300 nm), and graphene were prepared by cleavage on another substrate covered with PMMA. Then, the chosen graphene crystal was transferred on top of the chosen hBN crystal. To this end, we used alignment procedures similar to those described in ref. [S1,S2]. Electron-beam lithography and oxygen plasma etching were employed to define a 10-terminal Hall bar (Fig. S1). The second, thinner hBN crystal (thickness d) was carefully aligned to encapsulate the Hall bar but leave the contact regions open for a later deposition of metal contacts. After this, the second graphene crystal was prepared and transferred on top of the encapsulated graphene device. This second layer was also patterned into another Hall bar device that was carefully aligned with the bottom graphene structure (with a typical accuracy of ~10 nm). Finally, Au/Ti contacts we fabricated by using e-beam lithography and evaporation. After each transfer step, the devices were annealed at 300°C in an argon-hydrogen mixture to remove polymer residues and other contaminants. Figure S1 shows an optical image of a completed DLG device with d ≈12nm.

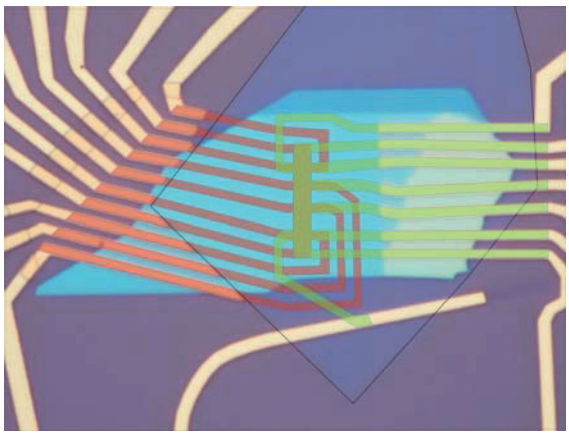

Figure S1. Double-layer graphene heterostructures. We use false colors to identify different layers in the heterostructure. The bottom graphene mesa is shown in false orange and lies on top of an opaque BN crystal (cyan to white is its natural color). A 12 nm hBN crystal resides on top of the graphene layer (transparent blue is its natural color but we added a thin black contour to identify the BN crystal's position). The top graphene layer is shown in false green. It is etched into the multiterminal Hall bar aligned with the bottom mesa. The width of the Hall bar is ≈2μm.

The exact thickness of the BN spacer was found retrospectively by using atomic force microscopy and capacitance measurements [S3]. Both techniques yielded the same value of d, which indicates the absence of any residue between the graphene layers (an extra monolayer of contamination would be detectable by this approach). Let us also stress the excellent insulating quality of hexagonal BN [S4], which allows a dielectric layer with d ≤4nm without any noticeable leakage current for gate voltages up to several V applied between the graphene layers [S2]. Such a separation between two-dimensional electronic systems is difficult if not impossible to achieve for GaAlAs heterostructures [S5].

#2 *Relation between gate voltages and induced carrier density*

In field-effect devices with a thick dielectric layer (e.g., using graphene on SiO_2), one can generally assume a linear relation $n \propto V_g$ between the induced carrier concentration n and gate voltage V_g. However, in our DLG heterostructures with an ultra-thin BN spacer the dependence becomes nonlinear due to quantum capacitance (QC) [S3]. Its contribution becomes particularly important in high-μ devices, in which one can approach close to the NP so that the density of states in graphene tends to zero [S3]. In our case of a double layer system, one needs to take into account that QC contributions come from both graphene layers, and this makes the relation between carrier densities in the control and studied layers (n_C and n_S, respectively) and applied voltages V_t and V_b particularly complicated and deserving a separate study.

To simplify our analysis in this work, we employed a constant capacitance approximation. To this end, we fixed V_t that induced charge carriers in the control layer, and determined n_C by using Hall measurements. Then, we swept V_b to change n_S in the studied layer (in the main text and below, we use notation n instead of n_S, unless this causes confusion). To convert V_b into n_S, we again measured the Hall effect away from the NP, typically at $|n_S| \approx 1$ to 5×10^{11}cm^{-2}. The inferred coefficient was used to translate V_b into n_S. The coefficient changed with varying n_C in the control layer. The latter was taken into account when the experimental curves were re-plotted in terms of n in the figures presented in this work.

The "linear approximation" assumes that QCs do not change significantly within the studied interval of n for a given n_C. As explained above, this is a simplification for a complex dependence of n_C and n_S as a function of V_t and V_b which is unique for every device [S3]. The approximation leads to deviations from the actual values of carrier concentrations in the two layers. We have found that deviations are relatively minor (typically, <20% for our range of studied n) and become significant only in the proximity of the NP where graphene's QC is minimal. In this regime, charge inhomogeneity is also significant (e-h puddles) which leads to a leveling-off of the decrease in QC. Furthermore, near the NP, we cannot determine n from Hall measurements because of charge inhomogeneity [S3], which makes it difficult if not impossible to improve further on the used linear approximation.

Despite some drawbacks, our approach is more meaningful than just quoting applied voltages that strongly vary for various devices, measurement configurations, etc. The linear approximation has no impact on any of the reported results, and all the curves remain qualitatively the same. However, if detailed analysis is needed, one has to keep in mind that the carrier densities n plotted in the main text are in fact scaled gate voltages, and there is some nonlinearity along the x-axis, which increases near the NP. When a better approximation is required (for example, to find μ; see below), we measured the Hall effect for every value of V_b to find n away from the NP.

#3 *Crosstalk between measurement current and effective gate voltage*

In DLG devices with nm-thin spacers, special care should be taken to avoid the influence of measurement current I on the induced carrier densities. Even for seemingly small currents I ~1nA, a voltage drop along the graphene device can reach into the mV range in the low-T insulating regime with high ρ (in the MOhm range). With reference to Fig. 1a, this voltage drop translates into an additional gate voltage ΔV_t that varies along the device. Unlike for the standard graphene devices with a thick dielectric, in our devices the effect of such an extra V_t is not negligible because of small d. For example, if $d \approx 4$ nm, 1mV of V_t translates into ~$5\text{x}10^9$ cm^{-2}, which is enough to shift the system away from the insulating state. For example, this can lead to an artifact of the resistance peak split into two. The crosstalk makes measurements in the insulating regime particularly difficult (Fig. S2).

To avoid artifacts in determining $\rho^{NP}(T)$ (insert in Fig. 2) we measured *I-V* curves at the NP at each *T* (see Fig. S2). Then, ρ^{NP} was defined from the linear part at $I \Rightarrow 0$. Because the range of the linear response shrinks with increasing ρ^{NP}, the crosstalk was probably responsible for some rounding of the curves at low *T*, which is seen in the inset of Fig. 2b. This is why we avoided the regime of low *T* and very high ρ^{NP}.

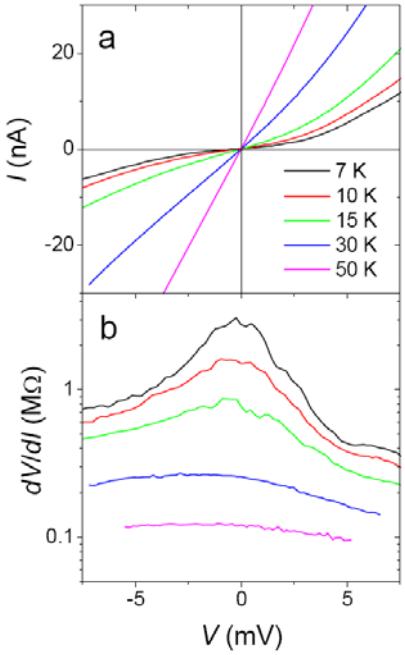

FIGURE S2. I-V characteristics in the insulating state for a device with *d* =4 nm. The nonlinearity in this state is mostly due to the crosstalk between the driving current and gate voltage. This was confirmed by studying changes in $\rho(n)$ with increasing *I* in different parts of the multiterminal devices, which caused different shifts of the NP as a local value of gate voltage varied by a few mV. (b) – Differential resistance for the curves in (a).

#4 Suppression of electron-hole puddles by doping of a nearby graphene layer

The suppression of e-h puddles in the studied graphene layer, when the control layer is set in a highly doped state, is an important notion that we used to explain the MIT transition. Although the idea is rather intuitive, we could confirm the suppression directly in an experiment. To this end, we monitored charge inhomogeneity in our DLG devices. The extent of the region with e-h puddles is often characterized by the width of the $\rho(V_g)$ peak [S6]. Our curves indeed become noticeably narrower at high doping of the control layer. However, to elucidate the broadening in more detail, it is useful to employ Hall measurements (Fig. S3). If graphene has only one type of charge carriers, its Hall resistivity follows the dependence $\rho_{xy} = 1/neB$ for both electrons and holes. The transition regime in which electrons and holes coexist (that is, e-h puddles coexist) corresponds to the region around the NP where ρ_{xy} as a function of electric doping changes its sign and reaches a maximum value, before following the $1/n$ dependence (Fig. S3). The width of this region is a good measure of charge inhomogeneity. The maximum value of ρ_{xy} is another way to judge the extent of e-h puddles' region. For graphene on hBN, the region of the coexistence of electrons and holes usually extends to several$\times 10^{10}$ cm^{-2} [S7] but this value corresponds to the disappearance of the deepest puddles. An onset of the MIT should probably be expected at lower *n* because of the required percolation.

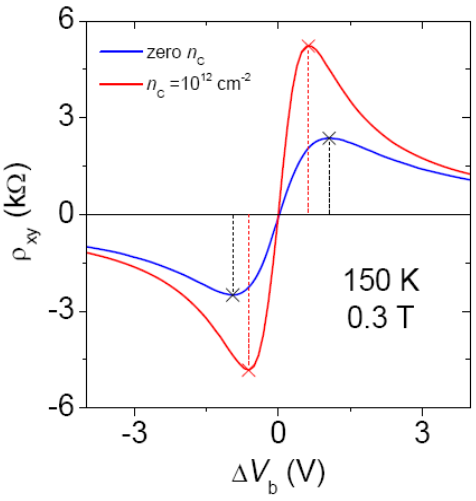

FIGURE S3. Typical changes in Hall resistivity of the studied layer with doping of the control layer. If the control layer is in its undoped state, the studied layer exhibits the behavior shown by the blue curve. Other examples of such curves and their analysis can be found in ref. [S7]. In the strongly doped regime ($n_C \approx 10^{12}$ cm^{-2}), the Hall curves become markedly sharper and the transition narrower (typically, by a factor of 2), which translates into twice shallower puddles. The data are for d =12 nm.

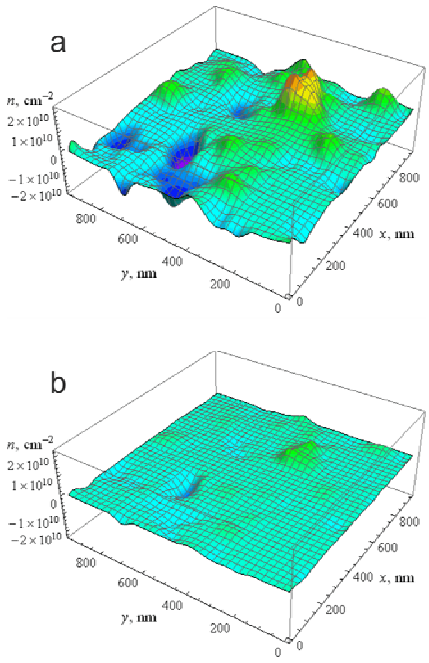

FIGURE S4. Simulated e-h puddles in the studied graphene layer for n_C = 0 and 5×10^{11}cm^{-2} (top and bottom panels, respectively).

In addition, we have modeled the suppression of e-h puddles in our geometry numerically, as shown in Figure S4. In these calculations, two graphene layers were assumed to be separated by d =4 nm and immersed in a dielectric media with ε ≈5. To mimic puddles, we have randomly distributed charged impurities in a concentration of 10^{10} cm^{-2} at a distance of 20 nm from the studied graphene layer,

which corresponds to a typical thickness of our BN substrates (see #1). The simulations were done by using the relativistic Thomas-Fermi model for graphene [S8]. Figure S4a shows the density fluctuations within a 1×1 μm^2 area of the studied layer in the absence of charge carriers in the control layer (zero n_C). One can see regions with large positive and negative densities (e-h puddles). The density variance δn in this case is found to be ≈8×10^9 cm^{-2}, where $\delta n^2 = 1/S \int n^2(\boldsymbol{r}) d^2 r$ and S is the area. For the strongly doped control layer (Fig. S4b), charge fluctuations in the studied layer become markedly weaker (δn ≈1×10^9 cm^{-2}).

The above simulations further support the idea that screening by the control layer is sufficient to suppress e-h puddles. Also, let us note that a metallic plate placed at distance d can wipe out only puddles with a typical size larger than d [S9]. Therefore, it was important that the control layer was placed as close as possible to the studied graphene layer, and this can explain why the MIT becomes less pronounced for the devices with large d. If a normal metal film is used instead of graphene, this should also suppress the puddles and allow the insulating state near the NP. The advantage of using graphene is that we can tune n_C and prove directly that the observed MIT is due to the conducting layer rather than changes in fabrication procedures and device's quality.

#5 *Reciprocity between top and bottom layers*

Although we have normally studied the bottom layer that was encapsulated in BN and showed high μ, the MIT could also be realized, if we swapped the studied and control layers. Fig. S5 shows an example of the MIT in the lower-μ top layer as a function of doping of the bottom layer. The transition is much less pronounced but, clearly, ρ^{NP} becomes larger with increasing $|n_C|$. This behavior is in agreement with our model for the MIT, that is, lower μ translates into deeper puddles that are harder to suppress by external screening.

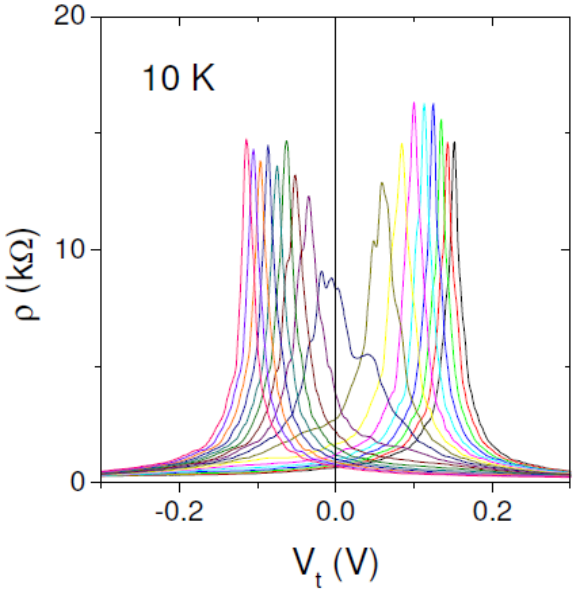

FIGURE S5. Resistivity of the low-μ top layer as a function of gate voltage V_t for different n_C in the bottom layer. n_C was varied by changing V_b in steps of 2V between -15 and +17 V (curves of different color). The device has the 4 nm spacer.

#6 ***Influence of external screening on charge carrier mobility***

The scattering mechanisms that limit charge carrier mobility in graphene remain debated and probably vary for different devices and substrates. Due to the possibility to partially screen out the Coulomb scattering potential in our DLG heterostructures, we can prove that there is more than one type of scatterers, at least, in our devices. For high-μ graphene (usually, the bottom layer), we find that μ significantly increases if a high density is induced in the top layer (upper panel in Fig. S6). This yields a significant role of Coulomb scattering in such graphene on hBN. On the other hand, for lower-μ graphene (usually, the top layer), we find little effect of n_C on μ, which suggests a non-Coulomb scattering mechanism.

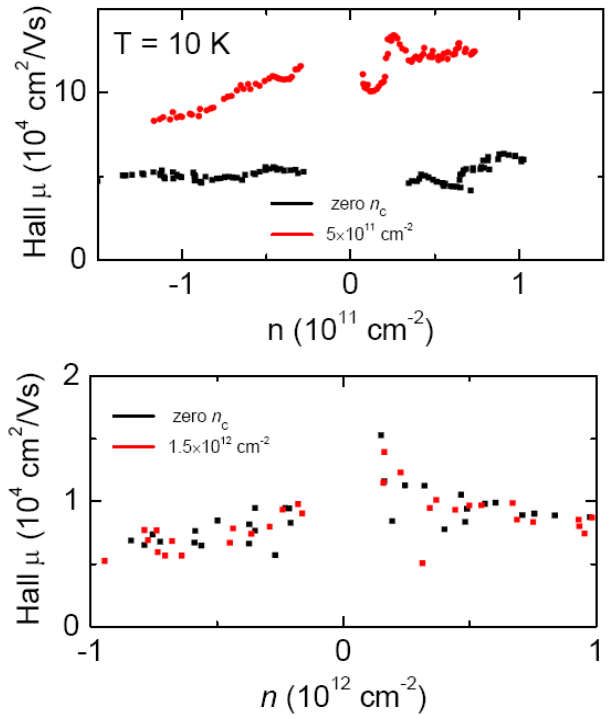

FIGURE S6. Changes in carrier mobility in the studied layer with doping of the control layer. High-μ layer is clearly sensitive to n_C, and its mobility increases from ~50,000 to 100,000 cm^2/Vs (top panel). No such changes were observed for low-μ graphene (μ~10,000 cm^2/Vs; low panel). In this case, we have chosen to present the data for the lowest μ observed in our DLG devices, which is similar to values for graphene on SiO_2. After several exposures to air and consecutive annealing, quality of graphene in the top layer gradually decayed from original μ ≥30,000 cm^2/Vs. The bottom layer was much more stable. Also, note that due to changes in quantum capacitance, the usual way of determining μ from the electric field effect (as $\sigma = ne\mu$) become unreliable and leads to significant errors in DLG devices (because n is no longer a linear function of gate voltage). Therefore, for better accuracy, we have determined n from Hall measurements in small B, which yields the Hall mobility instead of the field-effect one.

The fact that the MIT in our devices is accompanied by a pronounced increase in μ (therefore, in the mean free path l) clearly distinguishes our observation from the conventional MIT. To the best of our knowledge, Anderson localization has never been reported with decreasing disorder. Such behavior is counterintuitive but consistent with the proposed model for the MIT.

Supplementary references

[S1] C. R. Dean *et al*, *Nature Nano*. **5**, 722 (2010).
[S2] A. S. Mayorov *et al*, *Nano Lett.* **11**, 2396 (2011).
[S3] L. A. Ponomarenko *et al*, *Phys. Rev. Lett.* **105**, 136801 (2010).
[S4] T. Taniguchi, K. Watanabe. *J. Crystal Growth* **303**, 525 (2007).
[S5] A. F. Croxall, K. Das Gupta, C. A. Nicoll, M. Thangaraj, H. E. Beere, I. Farrer, D. A. Ritchie, M. Pepper, *Phys. Rev. Lett.* **101**, 246801 (2008); J. A. Seamons, D. R. Tibbetts, J. L. Reno, M. P. Lilly, *Appl. Phys. Lett.* **90**, 052103 (2007).
[S6] K. S. Novoselov *et al*, *Nature* **438**, 197 (2005).
[S7] D. A. Abanin, R. V. Gorbachev, K. S. Novoselov, A. K. Geim, L. S. Levitov. arXiv:1103.4742 (to appear in *Phys. Rev. Lett*. 2011).
[S8] D. P. DiVincenzo, E. J. Mele. *Phys. Rev. B* **29**, 1685 (1984).
[S9] L. A. Ponomarenko *et al*. *Phys. Rev. Lett.* **102**, 206603 (2009).